

Joint PP-PS inversion at Pikes Peak oil field, Saskatchewan

Hongbo Zhang, Gary F. Margrave, and R. James Brown

ABSTRACT

The method of simultaneous PP-PS inversion has recently been developed and tested on the 3D Blackfoot seismic dataset. This paper shows the application of this method on 3C-2D seismic data from Pikes Peak oil field. The inversion was accomplished with a newly installed inversion module in ProMAX. After careful prestack processing was done, five limited-offset stacked sections for each of the vertical and radial components were created, migrated, and correlated. The inversion module assumes that the data has been trace equalized and, to restore the average AVO behaviour, requires the input of scalar RMS amplitude estimates for each offset. These were obtained by creating elastic synthetic seismograms for P-P and P-S from well control and calculating the RMS amplitudes for each offset. Then the ten datasets, together with the RMS amplitude values, and a background velocity model were input into the joint PP-PS AVO-inversion module in ProMAX. The weighted stacking requires estimation of the P-P and P-S incidence angles at each depth level and this is done by raytracing through the background velocity model. Four attributes were determined: fractional P-wave impedance, fractional S-wave impedance, fractional $\lambda - \rho$, and fractional $\lambda - \mu$. Good correlation of these parameters from seismic inversion and those calculated from well logs shows that simultaneous PP-PS AVO-inversion can be used to indicate anomalous lithology and pore-fluid changes in the subsurface. Therefore it should be helpful in detecting hydrocarbons using 2D multicomponent seismic data.

INTRODUCTION

Geology

Pikes Peak oil field is a heavy-oil field located 40 km east of Lloydminster,

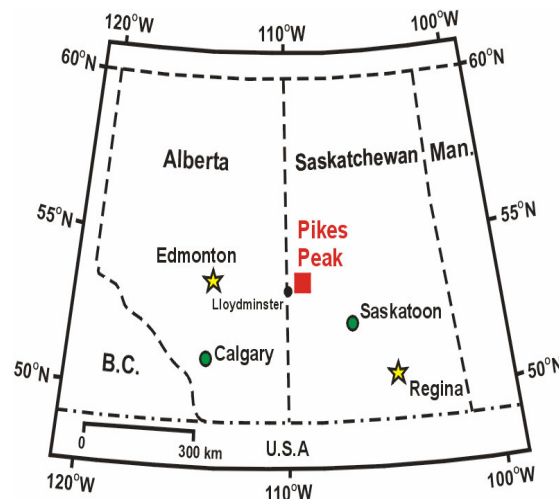


FIG. 1. Location map of the Pikes Peak oil field (edited from Hoffe et al., 2000).

Saskatchewan (Figure 1). It has been operated by Husky Energy Ltd. since 1981 and over 35 million barrels have been produced. Steam-drive technology has been used to enhance recovery. The principle of steam drive is to reduce the effective viscosity of the oil and increase the mobility in the reservoir by injecting steam at high-temperature and-pressure.

The producing reservoir is the Waseca Formation in the Lower Cretaceous. The sands and minor shale interbeds are outlined in light shades (Figure 2). At Pikes Peak, the Waseca Formation is 486 m below the surface of the Earth. The depositional environment is an incised valley filled with estuarine deposits of a basal homogeneous sand unit (Waseca sand), a sand and shale interbed unit (Waseca interbed), and a capping shale unit (Waseca shale; Van Hulten, 1984). The main producing zone within the Waseca Formation is the homogeneous sand unit. It ranges between 5 and 30 m of net pay within the field. Dissolution of deep Devonian salt units around the flanks of the field set up the combination structural and stratigraphic trap (Van Hulten, 1984).

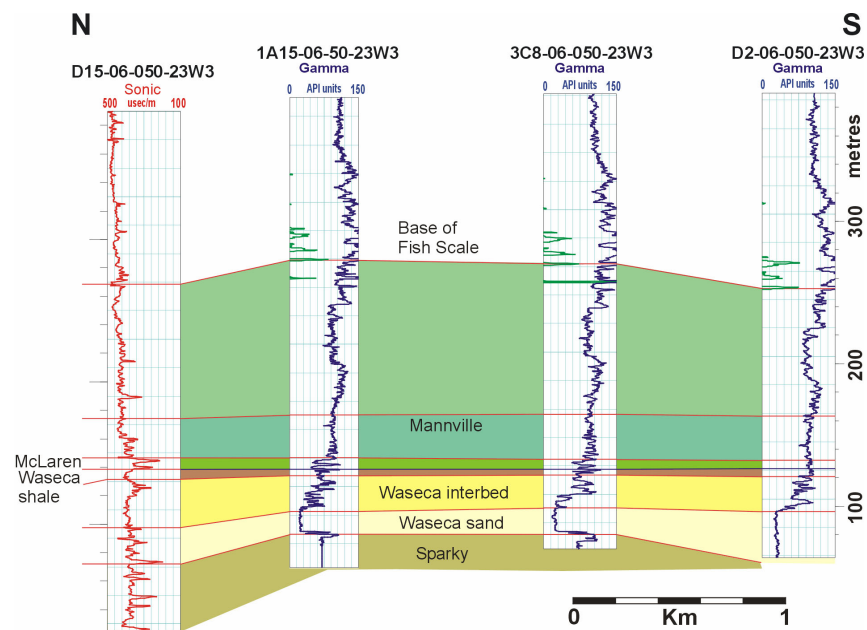


FIG. 2. Well-log cross-section illustrating the Lower Cretaceous stratigraphy (flattened at the top of the Waseca Formation). There is a channel sequence previously interpreted within the Waseca Formation (Van Hulten, 1984) and refined by the authors.

Methodology

The technique of joint PP-PS weighted stacking is used in the course of inversion. Stewart (1990) developed this method and Larsen and Margrave (1998), Larsen (1999), and Margrave et al. (2001) provided its first practical applications. The method requires migrated common image-point gathers for both P-P and P-S reflections. These are then summed into a weighted stack, where the weights are derived from a smoothed background velocity model, to estimate fractional P and S impedance. The resulting sets of stacked sections are estimates of changes in P-wave impedance and S-wave impedance. From these weighted stacks, such useful elastic parameters as fractional $\lambda - \rho$ and $\lambda - \mu$ can be derived. For the mathematical basis of this method, we refer to Larsen (1999).

The physical basis for the method is embodied in the first-order Zoeppritz-equation approximations for plane-wave reflection and transmission coefficients. The approximations are made under the assumptions that two solid half-spaces are welded at an elastic interface, that there are only small relative changes in elastic parameters, and that the average P- and S-wave angles of incidence and transmission across the interface do not approach a critical angle or 90° (Aki and Richards, 1980). The plane-wave assumption is one that can cause inaccurate estimation of near-offset data.

The implementation of this method can be generalized as follows. Firstly, the 3C-2D seismic data were acquired and processed to obtain high-quality, true relative-amplitude prestack seismic data volumes. Rather than performing a full prestack migration, these volumes were NMO-corrected and stacked into limited-offset volumes that could be post-stack migrated. Five of such limited-offset, migrated sections were created for both P-P and P-S reflections. Because true-amplitude recovery in regular processing is not perfect, synthetic seismograms for each reflection type were used to restore the average behaviour of reflectivity with offset. These were constructed from well logs by raytracing for the traveltimes and using the Zoeppritz equations for the reflection calculations. They were then band-limited to the recovered signal band of the data. Then the expected RMS amplitude for each offset range was calculated from the P-P and P-S synthetic seismograms. Each limited-offset migrated data volume was then rescaled by a constant factor to have the same RMS amplitude as the corresponding synthetic seismogram. Secondly, offset ranges were chosen to create limited-offset stacked sections so that the amount of data needed for AVO analysis would be decreased and both the speed of calculation and the signal-to-noise ratio would be increased. Since migration was also applied to the stacked sections, the quality of imaging was greatly improved. Thirdly, P-P and P-S reflection events were correlated in depth by comparing them to the synthetic seismograms. The data were then shifted to a common datum, just above the zone of interest, to restore the original depositional environment and reduce the errors in the inversion. Finally, each offset data volume is weighted and they are summed together to estimate fractional P or S impedance. For example, the fractional P-wave impedance is given by:

$$\frac{\Delta I}{I} = \sum_{offset} data \times weights, \quad (1)$$

where the sum includes both P-P and P-S data, the weights are functions of the average incidence and reflection angles for smooth P-wave and S-wave velocity-depth models, and where raytracing is used to determine the incidence, reflection, and transmission angles. The formulae for the weights are quite complex and are not reproduced here. They may be found in Larsen (1999).

The software that carries out the simultaneous PP-PS inversion is a module called joint P-P and P-S AVO inversion in ProMAX created by X. Li in 2000 and updated and documented by D. Henley in 2002. Software packages, SYNTH and LOGEDIT in MATLAB, were used to create the synthetic seismograms; Well Editor, GeoGraphix, Model Builder, and CorelDraw were also used in the course of this research and the composition of this paper.

DATA PREPARATION FOR JOINT PP-PS AVO INVERSION

Seismic processing

The seismic data used in this inversion project were acquired on the eastern side of the field (Figure 3) in March 2000 by the University of Calgary AOSTRA (Alberta Oil Sands Technology Research Authority) group and Husky Energy Ltd., and processed at Matrix Geoservices Ltd. For the vertical- and radial-component data used in this project, the processing from offset arrangement to inversion was performed by the authors and the processing before this was carried out by Matrix Geoservices Ltd. (Figure 4).

While the seismic data were being acquired, pump jacks for hydrocarbon production were running constantly. The noise from pump jacks does not show up in the vertical-component data because of its high frequencies (2-150 Hz). But the noise does show up in the radial-component data due to its much lower frequencies (2-60 Hz). This is why an $f-k$ filter was applied to the radial component. Careful attention was also paid to the large receiver statics present in the radial-component dataset. To solve this problem, the common-receiver stack was created so that the reflectors with small lateral changes were corrected. After that, residual source and receiver statics were calculated and eliminated.

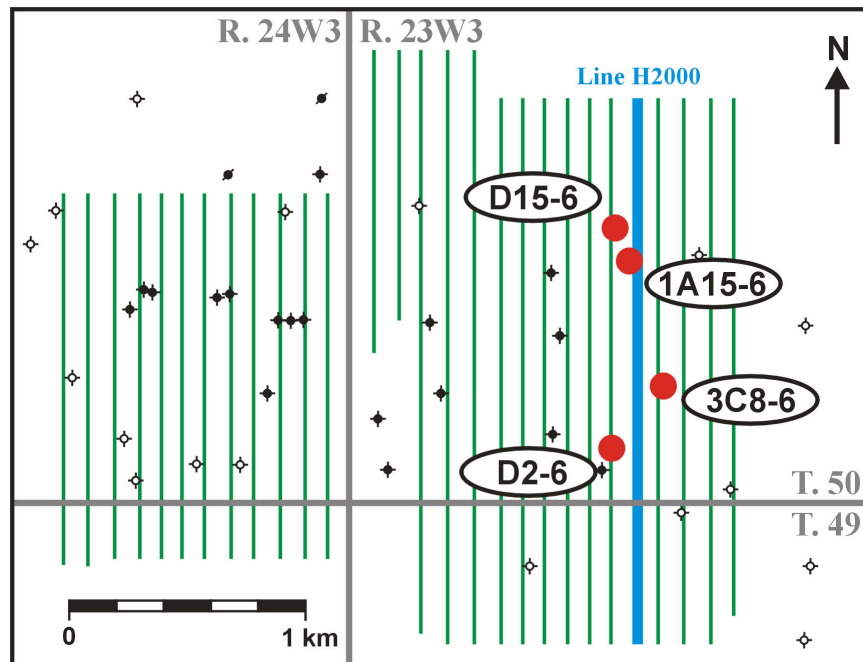


FIG. 3. Location map of the seismic line and the four wells used in this project.

The wells 1A15-6, D15-6, 3C8-6, and D2-6 were used to create synthetic P-P seismograms to tie to the P-wave seismic data due to the fact that they had original sonic and density logs over the Waseca interval. Well 1A15-6 was also used to tie to the converted-wave (P-S) seismic data because it had a dipole sonic log. For these data, a constant-phase rotation of -45° was applied to both the vertical- and radial-component data so as to give an optimal match to the synthetics (Figure 5).

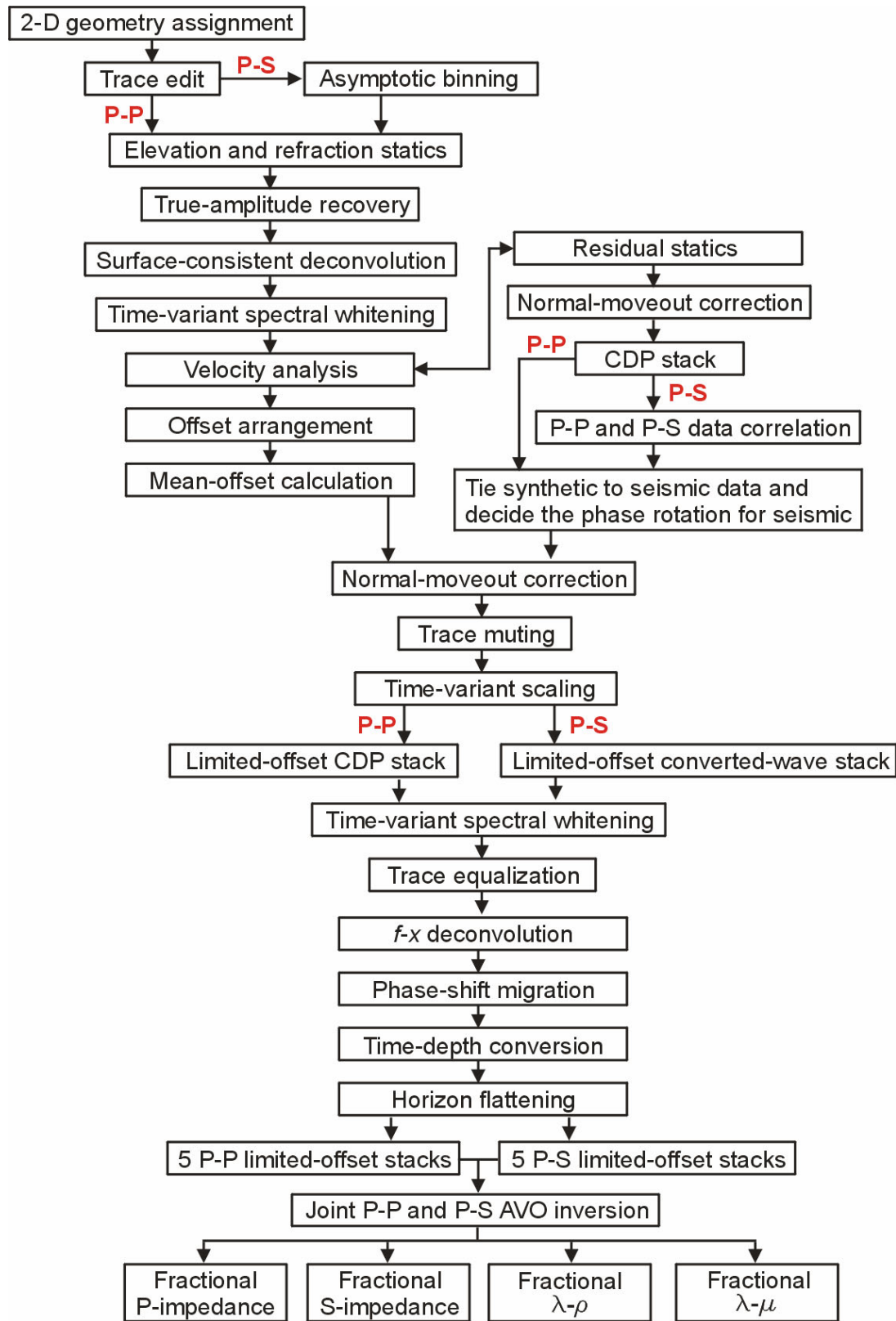


FIG. 4. Workflow for data preparation and joint PP-PS AVO inversion. Offset arrangement is the start of the processing by the authors. The process before offset arrangement was done by Matrix Geoservices.

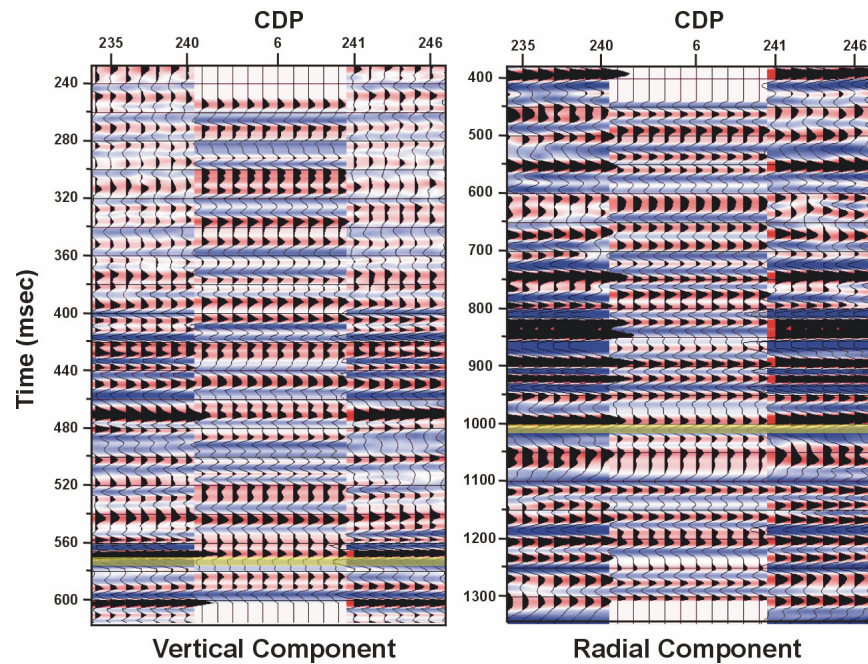


FIG.5. Synthetic seismograms for well 1A15-6 are both first of normal polarity, then rotated 45° and are tied with the vertical- and radial-component datasets. The Waseca top is at 570 ms and 1010 ms.

Event correlation

After all the static corrections were carried out on both the vertical and radial components, event correlation was the next important step in preparing for the joint inversion. The main purpose of event correlation is to restore the top of the zone of interest to the original deposition surface by flattening the datum horizon and reduce errors in the inversion.

The first step is to pick a common, easily identifiable regional horizon that is relatively free of thin-bed tuning effects or phase distortions above the presumed channel zone. An obvious horizon can improve picking accuracy. In this study, the top of the Waseca Formation was picked.

The second step is to convert P-P and P-S limited-offset data from the time domain to the depth domain using interval velocities calculated from P-P and P-S stacking velocities. The inversion is carried out in the depth domain.

The third step is to flatten both P-P and P-S limited-offset depth sections relative to the horizon obtained in step 1 and shift the flattened horizon to the corresponding depth in the well, the calculated attributes of which will be compared to the seismic inversion.

The fourth step is to output limited-offset sections relative to the flattened horizon for later use in the joint inversion.

Restoration of average P-P and P-S reflection behaviour with offset

True amplitude recovery during seismic processing is not perfect for AVO analysis. In fact, trace-equalization is almost always required before stacking so the extremely strong noise does not dominate the stack. This is not a great problem for P-P AVO analysis because the average AVO behaviour is nearly constant. However, for P-S data the average AVO behaviour is roughly sinusoidal with zero at zero offset and a maximum at some intermediate offset. Hence, it is necessary to attempt to restore the average AVO. For this purpose, synthetic seismograms were generated by raytracing for the traveltimes and using the Zoeppritz equations for the reflection strength. The inputs for these seismograms were well logs from the field and the final seismograms were band-limited to match the processed seismic data. The RMS amplitude at each offset range was calculated to obtain the average expected normalized amplitude values. The processed data were then adjusted to have the same RMS amplitude by multiplication by a different scalar for each offset. The synthetic P-P and P-S seismograms were made from the dipole well 1A15-6 at each offset range (Figure 6). Because the hydrocarbons in the zone of interest cause dramatic changes in velocity and density, only the parts above the production zone in each sonic and density log were used in the RMS amplitude calculation. Fractional P-wave and S-wave impedances were then weighted and inverted as shown in equations (2) and (3). The attributes fractional $\lambda - \rho$ and fractional $\lambda - \mu$ can be expressed in terms of the fractional P-wave and S-wave impedance as given by equations (6) and (7) (from Goodway et al., 1997).

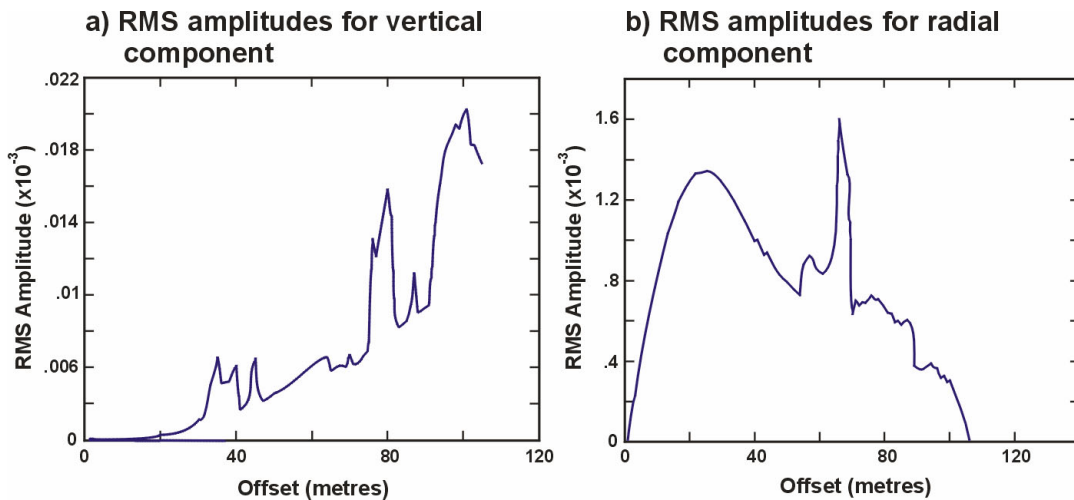


FIG. 6. RMS amplitudes versus offsets for (a) vertical and (b) radial components.

Calculation of the fractional P and S impedances

Fractional P-wave and S-wave impedance formulae are:

$$\frac{\Delta I}{I} = \sum_{\text{offset}} \left[W_{PP\frac{\Delta I}{I}}(\theta_{PP}, \varphi_{PP}) R_{PP}(\theta_{PP}) + W_{PS\frac{\Delta I}{I}}(\theta_{PS}, \varphi_{PS}) R_{PS}(\theta_{PS}) \right] \quad (2)$$

and

$$\frac{\Delta J}{J} = \sum_{\text{offset}} \left[W_{PP\frac{\Delta J}{J}}(\theta_{PP}, \varphi_{PP}) R_{PP}(\theta_{PP}) + W_{PS\frac{\Delta J}{J}}(\theta_{PS}, \varphi_{PS}) R_{PS}(\theta_{PS}) \right] \quad (3)$$

where θ_{PP} is the average of P-wave angle of incidence and reflection; φ_{PP} is P-wave angle of transmission; θ_{PS} is the average of P-wave angle of incidence and S-wave angle of reflection and φ_{PS} is S-wave angle of transmission. $W_{PP\frac{\Delta I}{I}}$, $W_{PS\frac{\Delta I}{I}}$, $W_{PP\frac{\Delta J}{J}}$ and $W_{PS\frac{\Delta J}{J}}$ represent the weights for P-P and P-S limited-offset stacks; R_{PP} and R_{PS} are, respectively, the observed P-P and P-S reflectivities, and $\frac{\Delta I}{I}$ and $\frac{\Delta J}{J}$ represent the fractional P-wave and S-wave impedances to be estimated.

CORRELATION OF SEISMIC INVERSION AND WELL LOG COMPUTATION

In this paper, in order to test whether the method of joint PP-PS AVO inversion is effective, especially the zone of interest shown in Figure 7, correlation of the results from seismic inversion and impedance estimates calculated from well logs was conducted.

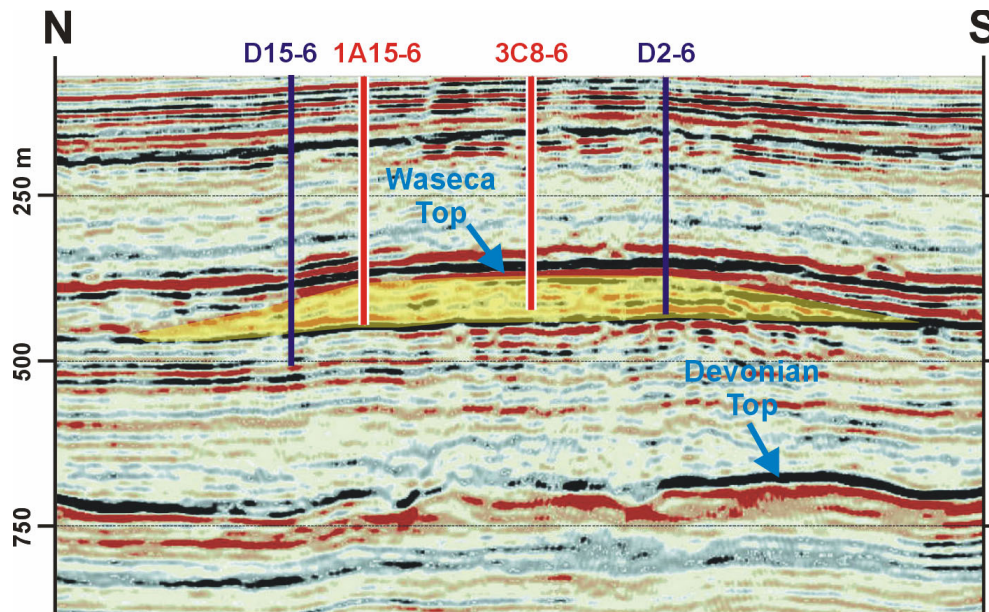


FIG. 7. The Waseca Formation reservoir and wells, including the dipole well 1A15-6 and well 3C8-6 (in grey) used in this paper.

Fractional impedance calculation from well logs

Since the frequencies of well-log data are much higher than those of seismic data, the well logs must be smoothed and downsampled (Figure 8) to be directly compared with

the seismic data. First, the well-log sampling interval (dz_2) is increased by local averaging and decimation. The well logs were averaged over 4-m and 2-m length scales for better P and S impedances correlation with the results from seismic inversion. Second, the fractional impedances (P and S) are generated from these downsampled data according to equations (4), (5), (6), and (7), by taking ratios of the difference and average of consecutive pairs of samples:

$$\text{Fractional P-wave impedance: } \frac{\Delta I}{I} = \frac{2(I_2 - I_1)}{I_2 + I_1}; \quad (4)$$

$$\text{Fractional S-wave impedance: } \frac{\Delta J}{J} = \frac{2(J_2 - J_1)}{J_2 + J_1}; \quad (5)$$

$$\text{Fractional } \lambda - \rho: \quad \frac{\Delta(\lambda\rho)}{\lambda\rho} = \frac{2}{\alpha^2 - 2\beta^2} \left(\alpha^2 \frac{\Delta I}{I} - 2\beta^2 \frac{\Delta J}{J} \right); \quad (6)$$

$$\text{Fractional } \lambda - \mu: \quad \frac{\Delta(\lambda/\mu)}{\lambda/\mu} = \frac{2\alpha^2}{\alpha^2 - 2\beta^2} \left(\frac{\Delta I}{I} - \frac{\Delta J}{J} \right); \quad (7)$$

where α and β are the average P-wave and S-wave velocities across the interface, $I = \rho\alpha$, $J = \rho\beta$. Equations (4) to (7), above, represent the formulae for fractional P-wave impedance, fractional S-wave impedance, fractional $\lambda - \rho$, and fractional $\lambda - \mu$.

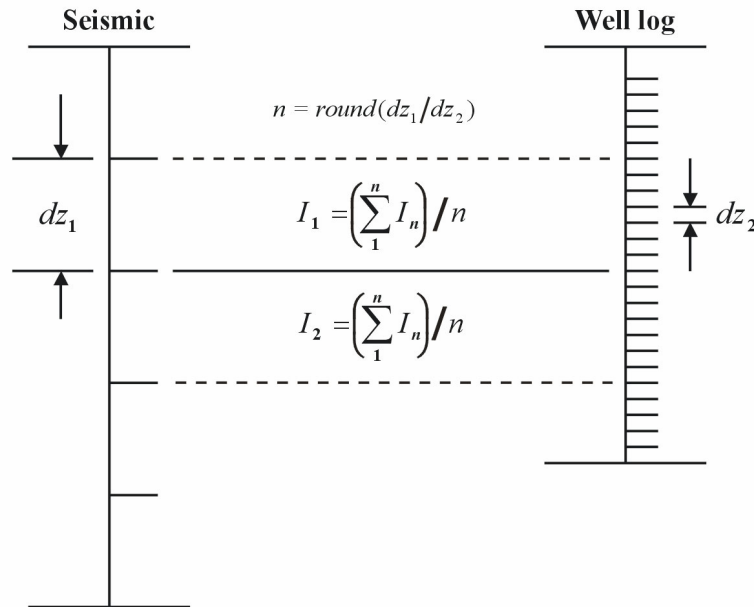


FIG. 8. An example of how the well log is downsampled to calculate fractional P-wave impedance.

Filtering of well-log computation

Despite the fact that the well logs were downsampled, the parameters calculated from the well logs have wider frequency band and much higher frequency content than those from seismic inversion. In order to correlate the well-log computation with the seismic inversion, band-pass filtering was done on the well-log computations by converting them to time using an average velocity. They were then converted back to depth after filtering.

Results of correlation

Generally, the correlation between seismic inversion and well-log computation for well 1A15-6 and 3C8-6 is quite good, especially within the zone of interest where there are hydrocarbons, although different sampling intervals were chosen and compared (Figures 9-12).

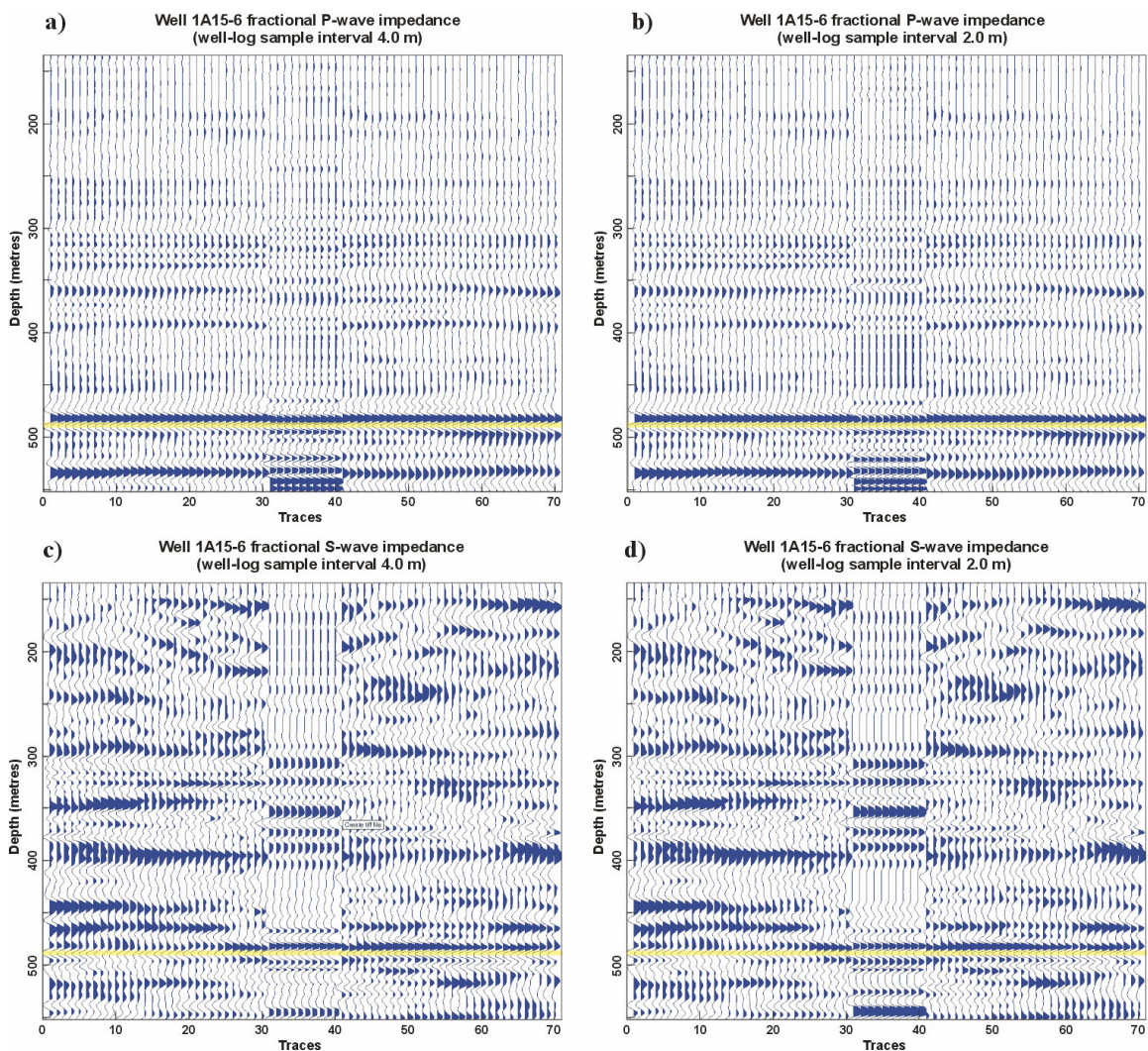


FIG.9. Well 1A15-6 correlation of fractional P-wave and S-wave impedance from seismic inversion and well-log computation, Waseca Formation top at 488 metre. Well log sample intervals of 4 metres (a and c) give better results than 2 metres (b and d).

Meanwhile, among the four attributes inverted for, fractional P-wave impedances and $\lambda - \rho$ are of higher frequencies and better imaging quality because they are more highly dependent upon P-P reflectivity. On the contrary, fractional S-wave impedances and $\lambda - \mu$ are of lower frequency because they are more dependent on shear impedance contrasts. In places where there are hydrocarbons, P-wave impedance and $\lambda - \rho$ change more than S-wave impedance and $\lambda - \mu$.

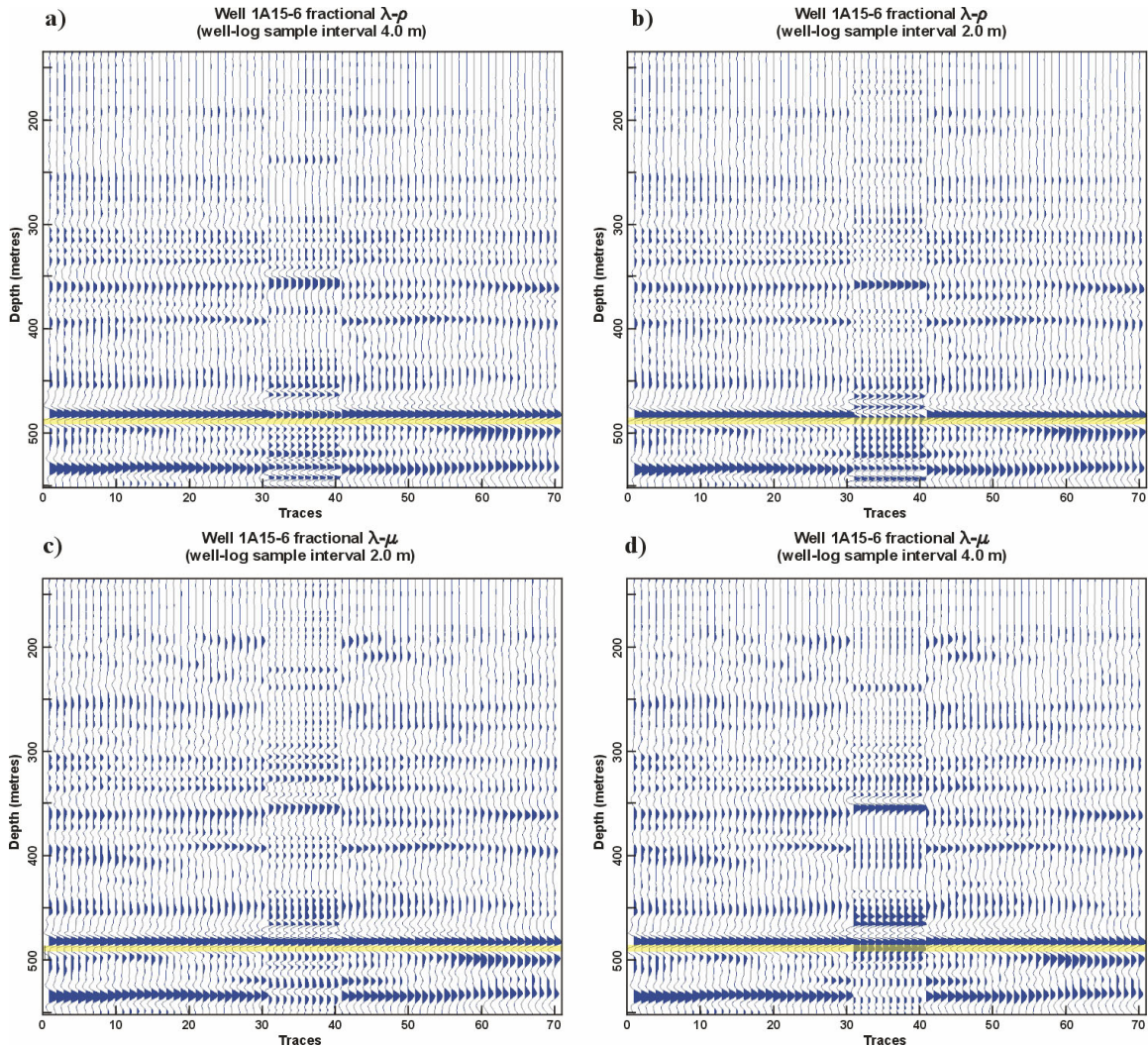


FIG.10. Well 1A15-6 correlation of fractional $\lambda - \rho$ and $\lambda - \mu$ from seismic inversion and well-log computation, Waseca Formation top at 488 metre. Well-log sample intervals of (a) and (c) yield better results than (b) and (d).

There are some misties between seismic inversion and well-log computation in either the shallow part or the part that is close to the datum. The latter may be due to phase differences between seismic and well-log computation and the steam-injection that was going on in other nearby wells. The former may be due to both lower fold for shallow seismic data and phase differences.

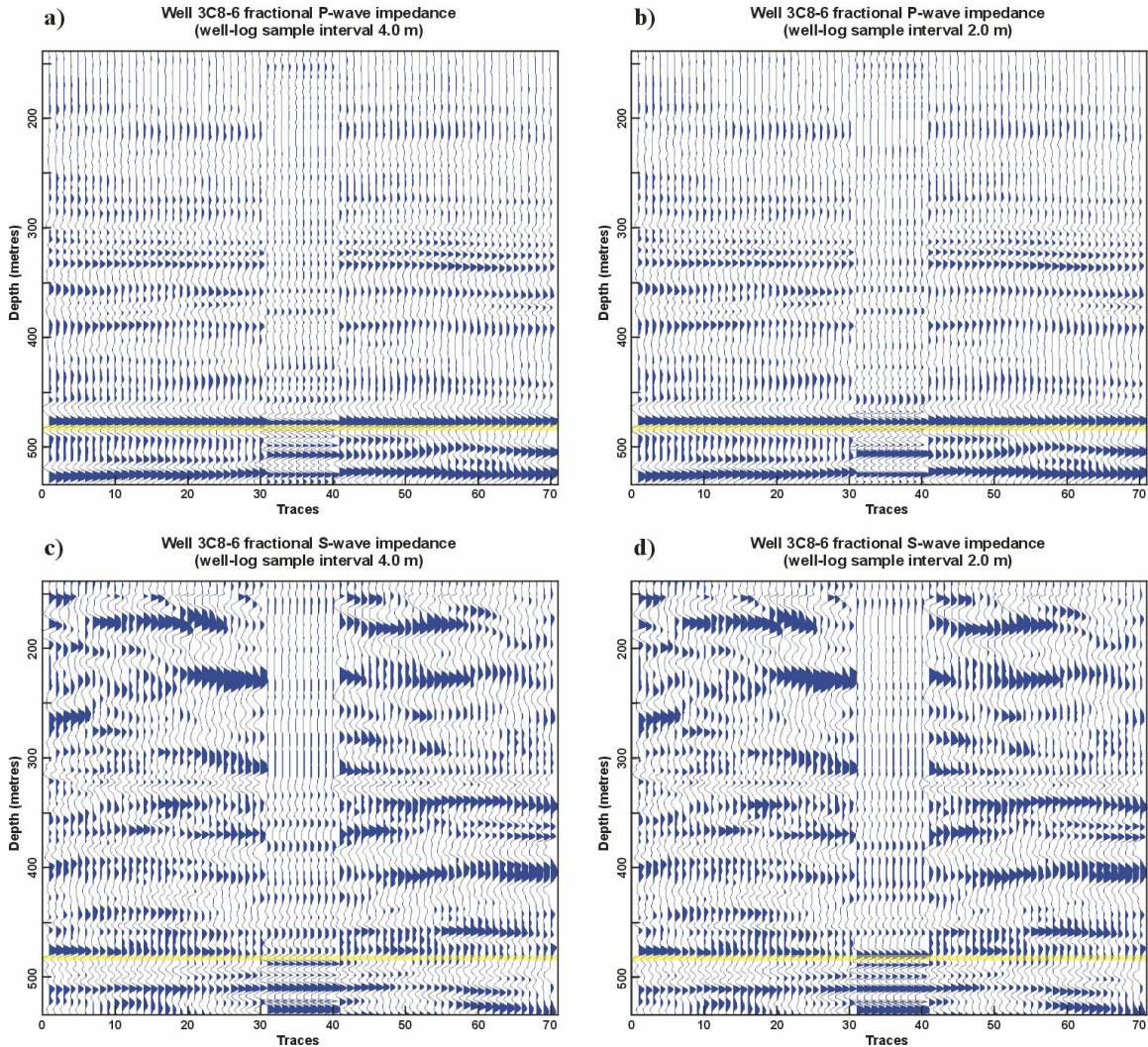


FIG.11. Well 3C8-6 correlation of fractional P-wave and S-wave impedances from seismic inversion and well-log computation, Waseca Formation top at 484 metre. Well-log sample intervals of 4 metres (a and c) give better results than 2 metres (b and d).

CONCLUSIONS

A joint P-P and P-S inversion was conducted on a 2D multicomponent seismic line over the Pikes Peak field. The inversion required forming migrated, limited-offset sections for both P-P and P-S data and creating synthetic seismograms from well control. Approximate relative amplitude restoration of the seismic data was accomplished by equalizing its RMS amplitudes with those of the synthetic seismograms for each offset. Then fractional P and S impedances were estimated by forming weighted stacks of the migrated, limited-offset sections. The success of the inversion was judged by comparing the estimated fractional impedances with direct calculations from wells.

By virtue of good correlation between seismic and well-log computation, it is concluded that the method of joint PP-PS AVO inversion worked well in this case. This could prove helpful in indicating anomalous lithology and pore-fluid changes in the

subsurface and, thereby, in oil and gas exploration, since information contained in both P-wave and S-wave seismic data is utilized in detecting these seismic anomalies.

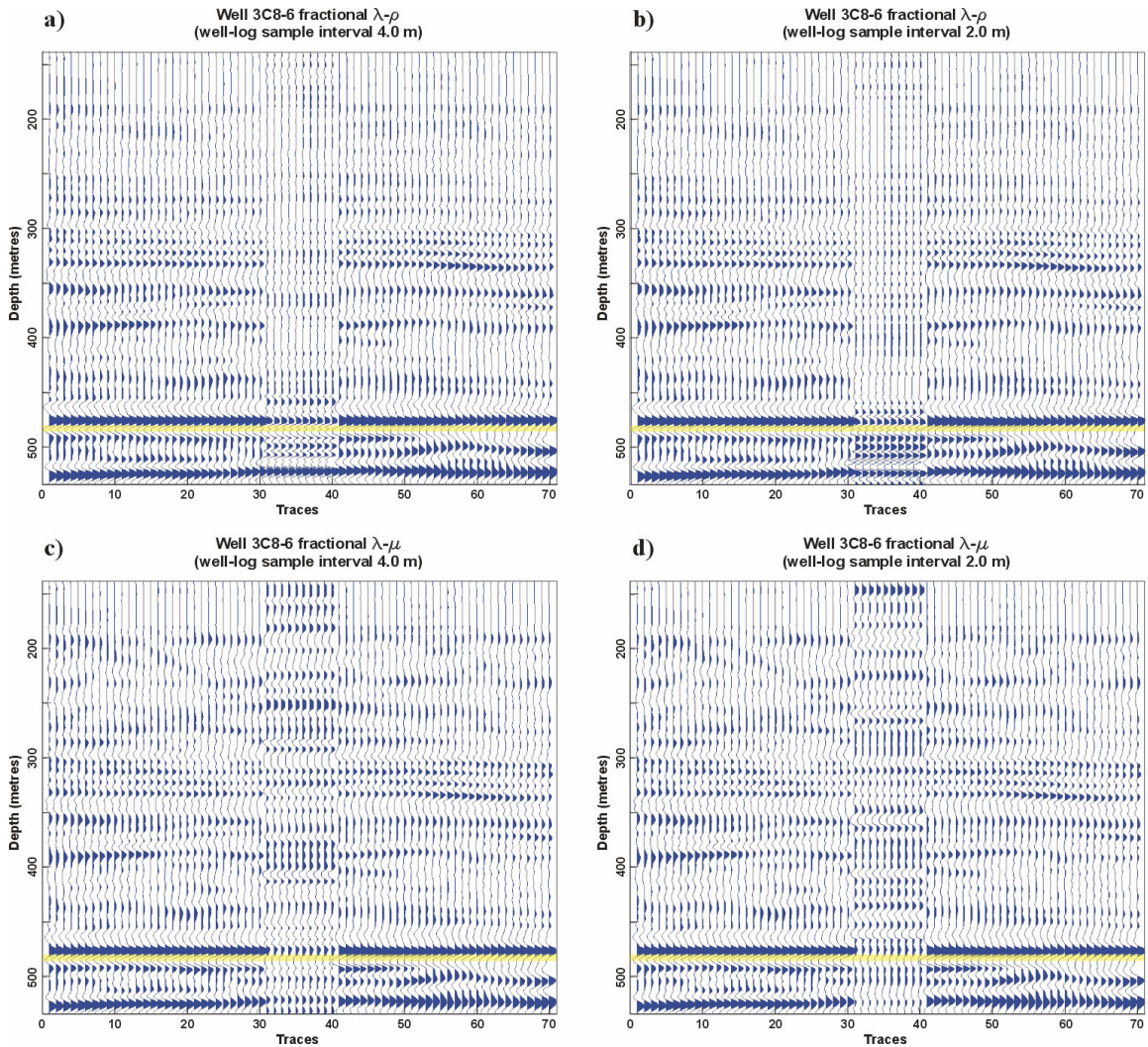


FIG.12. Well 3C8-6 correlation of fractional $\lambda - \rho$ and $\lambda - \mu$ from seismic inversion and well-log computation, Waseca Formation top at 484 metre. Well-log sample intervals of 4 metres (a and c) yield better results than 2 metres (b and d).

ACKNOWLEDGEMENTS

The authors gratefully acknowledge the support of the CREWES sponsors and discussions with Hanxing Lu, Dave Henley, Kevin Hall, and Ian Watson.

REFERENCES

- Aki, K. and Richards, P.G., 1980, Quantitative Seismology: Theory and Methods: W.H. Freeman and Company, Vol. 1.
- Goodway, B., Chen, T., and Downton, J., 1997, Improved AVO fluid detection and lithology discrimination using Lamé petrophysical parameters: “ $\lambda\rho$ ”, “ $\mu\rho$ ” and “ $\lambda\mu$ fluid stack”, from P and S inversions: CSEG Expanded Abstracts, 148-151.
- Henley, D.C., Margrave, G.F., and Zhang, H., 2002, Preparing input data for joint PP/PS inversion, CREWES Research Report. Vol. **14**
- Hoffe, B.H., Bertram, M.B., Bland, H.C., Gallant, E.V., Lines, L.R., and Mewhort, L.E., 2000, Acquisition and processing of the Pikes Peak 3C-2D seismic survey, CREWES Research Report, **12**, 511-522.
- Larsen, J.A., Margrave, G.F., Lu, H., and Potter, C.C., 1998, Simultaneous P-P and P-S inversion by weighted stacking applied to the Blackfoot 3C-3D survey, CREWES Research Report, **10**, 50, 1-23.
- Larsen, J.A., 1999, AVO inversion by simultaneous P-P and P-S inversion: M.Sc. Thesis, University of Calgary.
- Margrave, G.F., Stewart, R.R., and Larsen, J.A., 2001, Joint PP and PS seismic inversion: The Leading Edge, **20**, 1048-1052.
- Stewart, R.R., 1990, Joint P and P-SV inversion: CREWES Research Report, **2**, 112-115.
- Van Hulten, F.F.N., 1984, Petroleum geology of Pikes Peak heavy oil field, Waseca Formation, Lower Cretaceous, Saskatchewan, Canadian Society of Petroleum Geologists, Memoir 9, 441-454.